IEEE Access
Multidisciplinary | Rapid Review | Open Access Journal

Received November 21, 2021, accepted December 14, 2021, date of publication December 20, 2021,
date of current version December 28, 2021.

Digital Object Identifier 10.1109/ACCESS.2021.3136596

A Third Harmonic Current Elimination Strategy for Symmetrical Six-Phase Permanent Magnet Synchronous Motor

YIXIAO FENG[1], YONG LIAO[1,2], AND XUEKE ZHANG[3]
[1]Department of Electrical Engineering, Chongqing University, Chongqing 400044, China
[2]State Key Laboratory of Power Transmission Equipment and System Security and New Technology, Chongqing University, Chongqing 400044, China
[3]Xinxiang Power Supply Company, State Grid Henan Electric Power Company, Xinxiang 453000, China

Corresponding author: Yixiao Feng (yixiaofeng@cqu.edu.cn)

ABSTRACT This paper mainly focuses on the third harmonic current suppression for symmetrical six-phase fault-tolerant permanent magnet synchronous motor drives. First, a brief motor model is established to analyze the source of the third harmonic current. Resonant controller is always appreciated in terms of harmonic current suppression. However, its performance is highly dependent on the precise motor speed, which makes it not suit for variable-speed applications. Fortunately, adaptive filter can skip this problem. Then a current controller based on the adaptive filter is designed to eliminate the third harmonic current. However, the dynamic response of the controller designed is unsatisfactory. Besides, the steady edge of the controller is rather narrow, which limits the operation range of the motor. Then some improvements are made to the structure of the controller as well as the adaptive algorithm. Finally, several groups of experiments are conducted to compare both steady performance and dynamic performance of the controller based on adaptive filter and the improved controller. The experiments results coincide with the analysis and several conclusions are drawn. Besides, the proposed controller also applies to the elimination of other harmonic currents.

INDEX TERMS Adaptive filter, current controller, harmonic suppression, least mean square.

I. INTRODUCTION

High reliability has been one of the most important features of modern motor drives in the recent few decades. Modular motor drives and multiphase motor drives are the two main solutions in terms of fault-tolerant control. Modular motor drives are famous for their simple control method when the motor operates under fault conditions. Modular motor drives closed the corresponding modular where fault appears to realize fault-tolerant control and this may generate asymmetric radial magnetic force. Besides, this control method also scarifies the torque production ability to some extent. As to the multiphase motor drives, the asymmetric radial magnetic force can be eliminated by choosing the proper winding arrangement. Besides, they offer higher fault-tolerant ability when compared with three-phase motor drives [1], [2]. Moreover, permanent magnet synchronous motors (PMSMs) are widely used in industrial applications for their high-power density, which makes multiphase PMSM a good choice for safety-critical applications [3], [4]. Among all the multiphase motor drives, Six-phase (6Ph) PMSM is one of the most interesting ones since it can take full advantage of the well-developed three-phase PMSM drives [5]. Moreover, it can also achieve the tradeoff between the hardware complexity and fault-tolerant ability of the system. Ref. [6] makes a detailed analysis about the fault-tolerant ability of three kinds of six-phase PMSMs shown in Fig. 1. The result points out that the symmetrical 6Ph motor with one isolated neutral point has the best performance on the assumption that the sum of phase current is equal to zero. In practice, this assumption is commonly met to ensure the stability of dc-link voltage and preserve the hardware configuration of the system [7]. Therefore, symmetrical 6Ph PMSM with one isolated neutral point is a promising choice in terms of fault-tolerant control.

However, this structure of motor and system provides a path for the third harmonic current when motor operates under healthy conditions. Though it is reported in [8], [9] that the torque production of the multiphase motor

The associate editor coordinating the review of this manuscript and approving it for publication was Zhuang Xu.

could be improved by injecting the third harmonic current. Nonetheless, this method only applies to some kinds of multiphase motors, e.g., five-phase, asymmetrical six-phase motors where the third harmonic space current can produce a rotating magnet motive force (MMF). As to the symmetrical six-phase motor drives, the MMF produced by the third harmonic space current is pulsating which brings six-times torque ripples. Considering this, it is necessary to eliminate the third harmonic current when motor is operated under healthy conditions. Besides, in order to further improve the fault-tolerant ability of the system, fractional slot concentrated winding (FSCW) is commonly adopted in motor design [10], [11]. This winding design is characterized by the high independence of each phase winding. On the other hand, the decoupling between *dq* space and the third harmonic space also disappears in the interior PMSM, which means that current of *dq* space can induce a third harmonic voltage on the third harmonic space and produces the third harmonic current consequently. On the contrary, the third harmonic current can also induce a 6^{th} harmonic voltage on *dq* space [12], [13]. Namely, it is more urgent for interior PMSM equipped with FSCW to eliminate the third harmonic current under healthy conditions.

Up to now, many control strategies aiming to eliminate harmonic current have been proposed and they can also be used in the elimination of the third harmonic current. A PWM modulation method based on the redistribution of zero voltage vector is proposed in [14]. This method can effectively reduce the third harmonic voltage produced by the inverter. Nonetheless, it cannot eliminate the harmonic current produced by the PM. Besides, a proportional-integral (PI) controller is used to output the given third harmonic voltage, which may degrade the control performance because PI controller cannot track the ac signal with zero steady error. Proportional-resonant (PR) controller famous for its perfect ability to track ac signals is used in [15], [16] to eliminate the harmonic current. In general, resonant controller is commonly realized by the method of two integrators and these two integrators should be discretized in real systems, which moves the resonant frequency away from the given value [17]. A compensation method is proposed in [18] to correct the deviation. However, the performance of this method is highly dependent on the precise of the speed detection because the resonant frequency as well as the compensation are all calculated by the electrical angular frequency. In fact, to realize the implementation of field-oriented control (FOC), the rotor position is detected via sensors [19]. The rotor speed can be acquired by taking the derivative of rotor position to time and then filtering by a low-pass filter, which can hardly avoid bringing errors [20]. This makes the PR controller more suitable for power grid rather than variable frequency applications. Quasi-PR controller is proposed to reduce the effect motor speed has on the PR controller [21]. However, it takes the expense of sacrificing the infinite gain at the resonant frequency, which results in a steady error. An all-pass filter is used in [22] to construct a pair of orthogonal signals and then the amplitude and phase of the third harmonic current can be got. PI controller outputs the amplitude of the given voltage and the phase of voltage is 90^0 ahead of the current. This method suffers from the same problem as the PR controller because rotor speed is used to construct the all-pass filter. Besides, it is impossible that the amplitude of the third harmonic current equals zero perfectly in real systems, which causes the fact that the output of the PI controller will rise with time and finally lose its function. vector PI (VPI) controller is proposed in [23]. Though it offers satisfactory performance in terms of harmonic current elimination, it only applies to applications where a pair of orthogonal axis exists, which is unsuitable for symmetrical 6Ph motors.

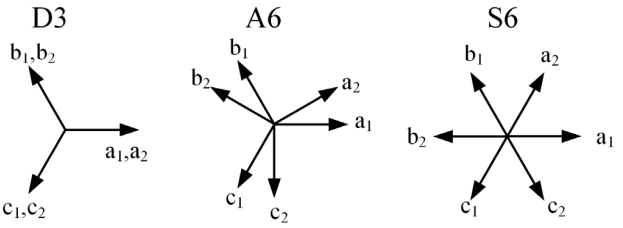

FIGURE 1. three kinds of six-phase motors.

The adaptive filter has been performing as a good technique in harmonic detection [24]. Moreover, it can also become a potential technique in harmonic elimination though there are still two barriers in front which are also the two objectives of this paper. In modern motor drives, a voltage source inverter (VSI) is commonly used to output the phase voltage. Then the first objective is how to get the given voltage when we get knowledge of the harmonic current. The least mean square (LMS) is widely used in the adaptive algorithm for its feature of simplicity [25]. However, the convergence rate of LMS is relatively low, which can hardly meet the command of motor drives. Therefore, the second objective is to improve the convergence rate of LMS.

This paper is organized as follows: the model of 6Ph PMSM studied is established firstly. The source of the 3^{rd} harmonic current is analyzed and the negative influence produced by the 3^{rd} harmonic current is also analyzed accordingly. Then by adjusting the structure of the adaptive filter, we can make the adaptive filter work as a current controller to eliminate the harmonic current. However, the dynamic performance of the controller is poor. Moreover, the steady edge of the controller is narrow, which limits the operation range of the motor. To solve this problem, by analyzing the iteration formula of the controller, an extra proportional factor is added into the iteration formula, which not only improves the dynamic performance of the controller but also broadens the steady edge of the controller. Finally, several groups of experiments are conducted to verify the effectiveness of the improved controller.

II. MODEL OF SIX-PHASE MOTOR CONSIDERING THE THIRD HARMONIC PM FLUX LINKAGE

The motor studied in this paper adopts fractional slot concentrated winding and PMs are embedded in the rotor. The motor is fed by a 6Ph power inverter. Moreover, the eddy effects, motor saturation and cogging effects are neglected when establishing the motor model.

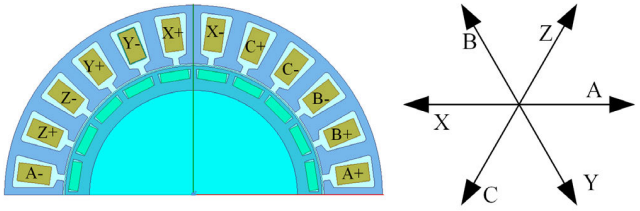

FIGURE 2. cross-section of the studied motor.

The studied 6Ph PMSM is shown in Fig. 2 which consists of two three-phase windings, i.e., the *ABC* winding and *XYZ* winding. There is a 60 electrical degree spatial shift between these two windings. This type of winding will produce fundamental, third, fifth, and seventh harmonic back electromotive force (EMF). However, this paper mainly deals with the elimination of the third harmonic current. Moreover, the proposed current controller also applies to the suppression of the fifth and seventh harmonic currents. Therefore, only the third harmonic permanent magnet flux is considered when modeling the 6Ph motor. The voltage and flux equation for the 6Ph PMSM at phase coordinate can be expressed as:

$$\begin{cases} U_s = R_s I_s + \dfrac{d\psi_s}{dt} \\ \psi_s = L_s I_s + \psi_{pm} \end{cases} \tag{1}$$

$$\psi_{pm} = \psi_{pm1}\begin{bmatrix} \cos\theta \\ \cos(\theta - 2\alpha) \\ \cos(\theta + 2\alpha) \\ \cos(\theta - 3\alpha) \\ \cos(\theta - 5\alpha) \\ \cos(\theta - \alpha) \end{bmatrix} + \psi_{pm3}\begin{bmatrix} \cos 3\theta \\ \cos 3\theta \\ \cos 3\theta \\ -\cos 3\theta \\ -\cos 3\theta \\ -\cos 3\theta \end{bmatrix} \tag{2}$$

$$L_s = diag\left(\begin{bmatrix} l_a & l_b & l_c & l_x & l_y & l_z \end{bmatrix}\right)$$

$$\begin{cases} l_a = l_x = l + l_2\cos(2\theta + 3\alpha) \\ l_b = l_y = l + l_2\cos(2\theta + 5\alpha) \\ l_c = l_z = l + l_2\cos(2\theta + \alpha) \end{cases} \tag{3}$$

where $R_s = \text{diag}[rrrrrr]^T$ is the phase winding resistance vector; ψ_{pm} represents the PM flux; ψ_{pm1} and ψ_{pm3} denote the amplitude of the fundamental and third harmonic PM flux respectively; θ indicates the rotor position (electrical); α equals to $\pi/3$ and

$$\begin{aligned} U_s &= \begin{bmatrix} U_a & U_b & U_c & U_x & U_y & U_z \end{bmatrix}^T \\ I_s &= \begin{bmatrix} I_a & I_b & I_c & I_x & I_y & I_z \end{bmatrix}^T \\ \psi_s &= \begin{bmatrix} \psi_a & \psi_b & \psi_c & \psi_x & \psi_y & \psi_z \end{bmatrix}^T \end{aligned} \tag{4}$$

are the arrays related to phase voltage, current, and flux. Due to the high independence of each phase winding, mutual inductance is relatively small and they can be ignored when modeling the motor. l represents the dc component of self-inductance and l_2 denotes the amplitude of the 2nd harmonic component of self-inductance.

According to the theory of space vector decomposition, the motor model under synchronous rotation frame, namely dq frame, can be got. The voltage equation and flux equation are shown in (5).

$$\begin{cases} U_{dq} = R_{dq} I_{dq} + \dfrac{d\psi_{dq}}{dt} - \omega T \psi_{dq} \\ \psi_{dq} = L_{dq} I_{dq} + \psi_{pmdq} \end{cases} \tag{5}$$

$$L_{dq} = \begin{bmatrix} L_1 & 0 \\ 0 & L_2 \end{bmatrix} \quad a_1 = \frac{1}{2}\ a_2 = \frac{\sqrt{3}}{2}\ a_3 = \frac{\sqrt{2}}{2}$$

$$L_1 = \begin{bmatrix} l - a_1 l_2 & 0 & -a_3 l_2 \cos 3\theta \\ 0 & l + a_1 l_2 & a_3 l_2 \sin 3\theta \\ -a_3 l_2 \cos 3\theta & a_3 l_2 \sin 3\theta & l \end{bmatrix}$$

$$L_2 = \begin{bmatrix} l & -a_3 l_2 \cos 3\theta & a_3 l_2 \sin 3\theta \\ -a_3 l_2 \cos 3\theta & l - a_1 l_2 & 0 \\ a_3 l_2 \sin 3\theta & 0 & l + a_1 l_2 \end{bmatrix} \tag{6}$$

where R_{dq} remains the same as R_s; L_{dq} represents the inductance matrix; T is a 6∗6 matrix, indicates the quasi-orthogonal property of the transformation matrix and can be expressed by (7):

$$T = \begin{bmatrix} T_{11} & 0 \\ 0 & 0 \end{bmatrix} \quad T_{11} = \begin{bmatrix} 0 & 1 \\ -1 & 0 \end{bmatrix} \tag{7}$$

Besides;

$$\begin{aligned} U_{dq} &= \begin{bmatrix} U_d & U_q & U_3 & U_0 & U_{z1} & U_{z2} \end{bmatrix}^T \\ I_{dq} &= \begin{bmatrix} I_d & I_q & I_3 & I_0 & I_{z1} & I_{z2} \end{bmatrix}^T \\ \psi_{dq} &= \begin{bmatrix} \psi_d & \psi_q & \psi_3 & \psi_0 & \psi_{z1} & \psi_{z2} \end{bmatrix}^T \end{aligned} \tag{8}$$

are the arrays related to the voltage, current, and flux; ψ_{pmdq} represents the PM flux in dq frame and can be shown as (9).

$$\psi_{pmdq} = \begin{bmatrix} \sqrt{3}\psi_{pm1} & 0 & \sqrt{6}\psi_{pm3}\cos(3\theta) & 0 & 0 & 0 \end{bmatrix}^T \tag{9}$$

$$U_3 = 3a_3\omega l_2\left(i_d \sin 3\theta + i_q \cos 3\theta\right) - 3\sqrt{6}\psi_{pm3}\sin 3\theta \tag{10}$$

$$u_{3d} = -a_3 l_2 \frac{d\,(i_3 \cos 3\theta)}{dt} \quad u_{3q} = a_3 l_2 \frac{d\,(i_3 \sin 3\theta)}{dt} \tag{11}$$

It can be inferred from (5), (6), and (9) that sources of the third harmonic voltage from machine side contains two portions just as shown in (10). The first is the third harmonic PM flux which is quite common in PM motors. The other is the coupled voltage produced by the dq axis current, which may account for most of the harmonic voltage especially under heavy load. Besides, due to the nonlinearity of the converter, there will be some harmonic voltage when outputting the phase voltage. Then the third harmonic current will flow in each phase winding. On the other hand, I_3 can also induce a sixth harmonic voltage in dq space just as shown in (11), which brings the sixth harmonic current and degrade the performance of the dq current controller. The bigger I_3 is, the bigger is the corresponding sixth harmonic current.

Therefore, it is necessary to eliminate the third harmonic current under healthy conditions. In terms of I_0, I_{z1} and I_{z2}, they are almost equal to zero in healthy conditions.

III. THE PROPOSED CURRENT CONTROLLER

As is known to all, PR controller shows potential in tracking ac signals. However, the resonant frequency bias caused by the discretization of the controller and the calculation error of the motor speed are the two main reasons for the poor performance of PR controllers. The former can be compensated on the condition that the motor speed is precisely detected. Consequently, the accuracy of motor speed is vitally important for the normal function of PR controller. Well, it is possible for the controller based on adaptive filter to skip this problem. To make it clear how the proposed controller works, a brief introduction of the adaptive filter is made first.

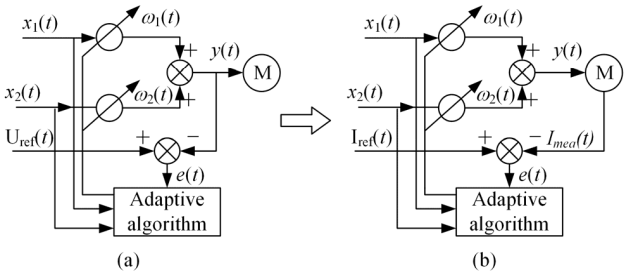

FIGURE 3. structure of (a) adaptive filter and (b) the proposed current controller.

A. STRUCTURE OF THE ADAPTIVE FILTER

The filter mainly consists of five portions, namely input, output, reference, tap weight and adaptive algorithm just as shown in Fig. 3. The main objective of the filter is to move the output close to the reference infinitely. When the filter works, according to the adaptive algorithm, tap weights are updated in each control cycle. When the filter reaches a steady-state, tap weight reaches its optimum. According to (10), it is reasonable to choose (12) as the input signal. It should be noted that (10) does not contain the third harmonic voltage produced by the inverter. Fortunately, it does not affect the performance of the filter. This is because its effect on the amplitude and phase of the third harmonic voltage can be compensated by changing the optimum of tap weight. The tap weight can be expressed as (13) then the output can be calculated by (14). As to the adaptive algorithm, the least mean square (LMS) is quite appealing for its feature of simplicity. The iteration formula of $\omega(t)$ can be expressed as (15).

$$x(t) = \left[\sin 3\theta \quad \cos 3\theta\right]^T \tag{12}$$

$$\omega(t) = \left[\omega_1(t) \quad \omega_2(t)\right]^T \tag{13}$$

$$y(t) = x(t)^T \omega(t) \tag{14}$$

$$\begin{cases} e(t) = U_{ref}(t) - y(t) \\ \omega(t+1) = \omega(t) - \dfrac{d\left(e(t)^2\right)}{d\omega(t)} = \omega(t) + 2\mu e(t) x(t) \end{cases} \tag{15}$$

where μ is the step size which has a great effect on the performance of the filter. When μ is set at a big value, the filter has a higher convergence rate but may diverge or have a big steady error. On the contrary, when it is set at a small value, the filter has a small steady error but takes the expense of losing a high convergence rate. It can be concluded that the selection of μ is rather contradictory. To ensure the stability of the filter, a new variable named $V(t)$ is introduced in (16) and it represents the difference between tap weight and its optimum expressed as $\omega_{opt}(t)$. Then $e(t)$ can be rewritten as (17). The iteration formula of $V(t)$ can be got just as shown in (18). If $V(t)$ attenuates in each cycle and finally converges to zero, it can be said that the filter is stable. Consequently, μ is constrained by (19). In addition, according to the LMS, $\omega(t)$ always moves to a point that can minimize $e(t)$. When there is no local optimum solution, $\omega(t)$ will finally reach $\omega_{opt}(t)$. The direction indicated by the brown line shown in Fig. 4 is commonly called the steepest descent direction, which is the tangent direction of the corresponding point. $\omega(t)$ will move in this direction by a distance decided by μ, which requires that μshould be bigger than zero. The superscript in Fig. 4 means two random $\omega(t)$.

$$V(t) = \omega_{opt}(t) - \omega(t) \tag{16}$$

$$e(t) = x(t)^T V(t) \tag{17}$$

$$V(t+1) = \omega_{opt}(t+1) - \omega(t+1) = (I - 2\mu\lambda) V(t)$$

$$\lambda = \max\left(x(t) x(t)^T\right) \tag{18}$$

$$|I - 2\mu\lambda| < 1 \; \lambda = \max\left(x(t) x(t)^T\right) \tag{19}$$

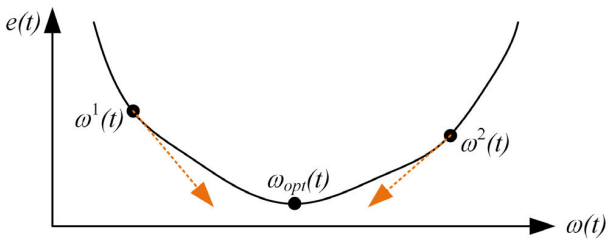

FIGURE 4. trajectory and move direction of ω(t).

B. CONTROLLER BASED ON LMS

We can get the exact harmonic voltage with (10) and then output a voltage with the same amplitude but antiphase to counteract this harmonic voltage, which finally eliminates the harmonic current. However, the calculation is parameter-dependent, which can hardly avoid bringing errors. Besides, the harmonic voltage produced by the inverter is not included in (10). Considering this, some changes are made to the structure of the filer just as shown in Fig. 3. Firstly, the reference signal is modified as the given current. the error signal can be expressed as (20) where $I_{mea}(t)$ can be easily calculated by the measured phase currents. It should be noted that $e(t)$ is no longer the difference between the reference and

the output of the filter, which differs the iteration formula of the controller from that of the filter.

$$e(t) = I_{ref}(t) - I_{mea}(t) \tag{20}$$

$$\frac{d(e(t))^2}{d\omega(t)} = 2e(t)\frac{de(t)}{dI_{mea}(t)}\frac{dI_{mea}(t)}{d\omega(t)} \tag{21}$$

$$I_{mea}(t) = \frac{y(t) + u_3(t)}{pl + r} \tag{22}$$

$$p = \frac{1 - z^{-1}}{T_s} \tag{23}$$

Before deducing the iteration formula of the controller, it is necessary to figure out the derivative of $e^2(t)$ to $\omega(t)$. Though $e(t)$ has no direct relation with $\omega(t)$, it is a function of $y(t)$ that creates the relation between $e(t)$ and $\omega(t)$ just as shown in (21). $I_{mea}(t)$ can be expressed as (22) where p is the differential operator. For the convenience of the implementation of the controller, the controller should be discretized. Backward Euler discretization is adopted in this paper and p can be replaced by (23) where T_s is the control cycle. z^{-1} represents one control cycle delay. Then $I_{mea}(t)$ can be rewritten as (24) where l_3 means the inductance of the third harmonic space and it is possible to figure out (21). It should be noted that (24) is only used for derivation. When calculating $e(t)$, $I_{mea}(t)$ can be calculated by the phase current detected by current sensors. It can be inferred from (10) that $u_3(t)$ is only concerned with the motor parameter and motor operation status, which makes the derivative of $u_3(t)$ to $\omega(t)$ lose its meaning. Besides, $I_{mea}(t\text{-}1)$ is a variable at time $(t\text{-}1)$. Therefore, the derivative of $y(t\text{-}1)$ to $\omega(t)$ has no sense. Then (21) can be figured out and expressed as (25). The iteration formula of the controller is shown in (26) and Fig. 5 shows this process.

$$I_{mea}(t) = k_1(y(t) + u_3(t)) + k_2 I_{mea}(t-1)$$
$$k_1 = \frac{T_s}{l_3 + rT_s} \quad k_2 = \frac{l_3}{l_3 + rT_s} \tag{24}$$

$$\nabla(t) = \frac{d(e(t))^2}{d\omega(t)} = \frac{-2e(t)x(t)T_s}{l + rT_s} \tag{25}$$

$$\omega(t+1) = \omega(t) - \mu\nabla(t) = \omega(t) + 2k_1\mu e(t)x(t) \tag{26}$$

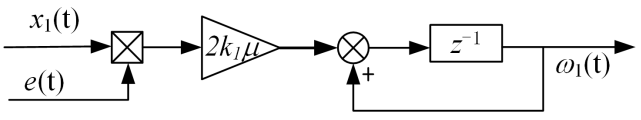

FIGURE 5. adaptive algorithm diagram of the controller.

When the controller works, $\omega(t)$ will preserve its value unless the motor status changes. At this time, a current error will appear, which indicates that the voltage output by the controller cannot counteract the harmonic voltage. Then $\omega(t)$ is updated according to (26) and the voltage output by the controller also changes. $\omega(t)$ will continue to adjust itself until it reaches its optimum. It should be noted that when the motor reaches another steady state, $\omega_{opt}(t)$ is uniquely decided according to (10) and local optimal solution does not exist, which ensures that $\omega(t)$ can finally converge to $\omega_{opt}(t)$. Meanwhile, the voltage output by the controller will counteract the harmonic voltage, thus eliminating the harmonic current.

Comparing (15) and (26), we can find that the whole iteration process of the filter and controller is near all the same. The introduction of the third harmonic space model seems to only bring a proportional factor which is decided by the motor parameter in the iteration formula. However, it also affects the value range of the μ. In order to make it clear the selection principle and the value range of μ. It is necessary to figure out the iteration formula of $V(t)$ for the controller. It should be noted that when the motor reaches a steady state, $u_3(t)$ is uniquely decided and the same goes for $\omega_{opt}(t)$.

$$\begin{aligned} V(t+1) &= \omega_{opt}(t+1) - \omega(t+1) \\ &= b_1 V(t) - b_2 e(t-1)x(t) \\ b_1 &= I - 2\mu k_1^2\lambda \quad b_2 = 2\mu k_1 k_2 \end{aligned} \tag{27}$$

In the same manner as described in the former section. $V(t)$ can be got and expressed as (27). Comparing (27) and (18), we can find that $V(t+1)$ of the controller contains two portions. The first portion, namely $b_1V(t)$ represents the self-attenuate of $V(t)$. The second portion, i.e., $b_2e(t\text{-}1)x(t)$ can be seen as the disturbance, which does not exist in (18). This means that if we choose the same μ for the controller and adaptive filter, the disturbance in $V(t)$ of the controller is bigger than that in the adaptive filer, which may cause instability of the controller. Then a smaller μ is appreciated to minimize the effect the disturbance has on the controller. In other words, though the iteration formula of $\omega(t)$ for the controller and adaptive filter is much alike, the change to the structure of adaptive filter influences the value range of μa lot. Besides, it is nearly impossible to figure out the analytical solution to $V(t+1)$ from (27) and the exact formula to decide the value range of μ. However, it does not matter the selection principle of μ, which are concluded in the following:

a) μ is bigger than zero to ensure the normal function of the controller.
b) In order to reduce the effect the disturbance has on the controller, b_2 should be as small as possible, which leads to a small μ.
c) The absolute value of b_1 should be smaller than 1 to ensure the stability of the controller. Besides, when b_1 is set at a small value, the controller has a high convergence rate and this can only be realized by choosing a relatively big μ.

Though there is no exact formula to definite the value range of μ given in this paper, the three principles give instructions about the selection of μ to ensure the stability of the controller. The first principle is decided by the theory of LMS, which ensures that $\omega(t)$ converges to $\omega_{opt}(t)$ step by step. If μ is negative, then $\omega(t)$ will move against the direction of the brown line pictured in Fig. 4, which causes that $\omega(t)$ will never converge to $\omega_{opt}(t)$ or even seriously leads to the

divergence of the controller. In terms of the 2nd principle, it is not really necessary for adaptive filter due to that the iteration formula of $V(t)$ in the filter does not contain the disturbance expressed in (27) at all. However, it does make help when it comes to the proposed controller because a smaller μ can help reduce the disturbance to the controller, which improves the stability of the controller. As to the last one, it can be inferred from (27) that it is vital for the controller to meet this principle. Otherwise, $V(t)$ will diverge to infinite, thus leading to the breakdown of the controller. In a word, the first and the last principle are two necessary principles that must be met. The 2nd principle is helpful to the stability of the controller. Except for these three principles, it is also available and necessary to decide the control parameter via simulations and experiments, which can further ensure the stability of the controller.

It can be concluded that the selection of μ is rather contradictory. If we want to get a high dynamic response speed, a relatively big μ is appreciated. However, this may cause the instability of the controller. If a small μ is chosen, the dynamic performance of the controller is poor.

C. THE IMPROVED CONTROLLER

For the convenience of selecting μ, a proportional factor named k_p is added to the adaptive algorithm just as shown in Fig. 6. k_p makes it much easier to achieve the tradeoff between the high convergence rate and the stability of the controller. From the macroscopic point of view, we can choose a big k_p and a small μ. k_p helps $\omega(t)$ converge to its optimum quickly, thus improving the dynamic performance of the controller. μ helps eliminate the steady error of the controller. However, it is not really true that the bigger k_p is, the better performance of the controller has. In order to make it clear the selection principle of k_p and μ, a detailed analysis is conducted in the following.

$$\begin{cases} \omega(t+1) = \omega_i(t+1) + k_p e(t) x(t) \\ \omega_i(t+1) = \omega_i(t) + 2\mu k_1 e(t) x(t) \end{cases} \tag{28}$$

$$\begin{aligned} V(t+1) &= b_1 V(t) - b_2 e(t-1) x(t) \\ &\quad + e(t-1)\left[k_p x(t-1) - k_2 k_p x(t)\right] \\ b_1 &= I - \left(2\mu k_1^2 + k_1 k_p\right)\lambda \quad b_2 = 2\mu k_1 k_2 \end{aligned} \tag{29}$$

The iteration formula of the controller is shown in (28). In the same manner as described in the previous section, the iteration formula of $V(t)$ can be got just as shown in (29). Comparing (29) and (27), we can find that an extra component appears, which can also be regarded as the disturbance. When the motor operates at a low frequency, $x(t)$ is nearly equal to $x(t\text{-}1)$. Then this disturbance is nearly zero on the addition that k_2 is approximate to 1. In fact, this condition is commonly met. On the one hand, the phase resistor can be ignored when compared with the phase reactance. On the other hand, the control frequency is commonly several times the motor operating frequency to ensure the normal function of the digital control systems. Then it can be inferred that k_2 is nearly 1 according to (24). Though b_2 remains the same as in the previous section, a constant decided by k_1 and k_p is added to the expression of b_1. Namely, a small μ is still in need to reduce the negative influence produced by the disturbance. However, we can adjust k_p to get better performance of the controller. Then the selection principle of k_p and μ can be got.

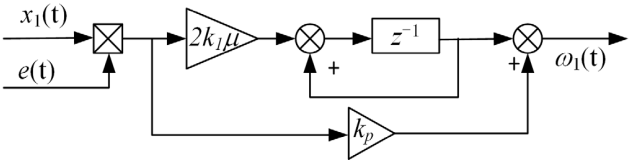

FIGURE 6. adaptive algorithm diagram of the improved controller.

a) k_p and μ are bigger than zero to ensure the normal function of the controller.
b) same as described in the previous section.
c) Similar with that described in the previous section. However, a relatively big k_p and a small μ is appreciated.

By comparing the principle in this section and section B, we can find that they are near the same. however, the parameter selection of the improved controller is much more flexible. On the one hand, a small μ can be set to ensure the stability of the controller. on the other hand, a big k_p can be chosen to get a high convergence rate. It should be noted that the selection of k_p and μ should be constrained by principles (a) and (c). When k_p equals zero, the improved controller is the same as the controller (traditional controller) described in section B.

IV. EXPERIMENT RESULT

In order to verify the effectiveness of the proposed current controller, some experiments are conducted. The motor parameters studied are shown in Table 1.

TABLE 1. Motor parameters.

symbol	Description	value
ψ_{pm}	Fundamental component of PM flux	0.0052 Wb
ψ_{pm3}	3rd harmonic component of PM flux	1.27e-5 Wb
l_2	2nd harmonic component of l_n	13 μH
l_0	Dc component of l_n	113.43 μH
r	Phase resistance	0.00935 Ω
P	Pole pairs	10
N	Slot number	24

Fig. 7 shows the whole control scheme, Where T_{62} indicates the coordinate transformation and $e^{j\theta}$ represents the inverse coordinate transformation. Under healthy conditions, I_{z1} and I_{z2} are nearly zero. Besides, the motor adopts one isolated neutral point, which makes I_0 always equal to zero. Therefore, there is no need to control the zero-sequence current.

The experiment set is shown in Fig. 8. Under the function of the six-leg inverter, the DC source provides power to

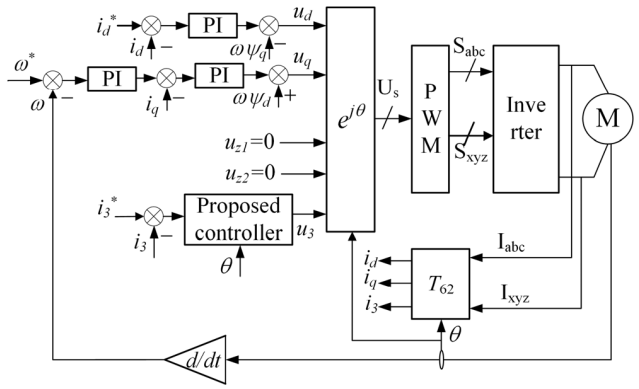

FIGURE 7. control frame of the whole system.

the studied 6Ph motor which drives the three-phase PMSM named as load motor in Fig. 8. The stator of the load motor is connected to one three-phase rectifier bridge which is finally connected to the DC load. The voltage of the DC source is set at 20V, the control period is 100 μs and the switching frequency is 10kHz.

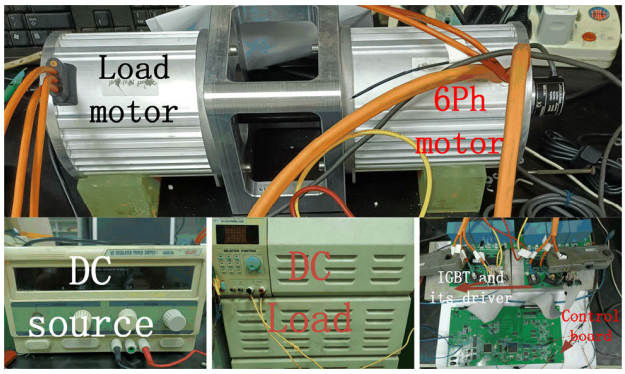

FIGURE 8. experiment set.

A. STEADY PERFORMANCE

For the convenience of description in the following, a new variable named k_i is defined and it is proportional to μ just as shown in (30). The studied motor is driven at 540rpm and I_d equals -15A. Then waveforms of I_a and I_3 under four different conditions are recorded and shown in Fig. 9. The first is under the condition where I_3 is without control. It can be observed that I_3 has an amplitude of nearly 5A under this condition. Then in the next two conditions, the I_3 controller based on LMS is enabled with k_i equal 0.003 and 0.0045 respectively. When k_i equals 0.003, I_3 is nearly zero and the waveform of I_3 is more sinusoidal compared with the first condition, which means that the controller based on LMS can eliminate I_3 under steady conditions. Besides, when k_i is smaller than 0.003, the controller can also eliminate the third harmonic current. In order to explore the biggest k_i available, k_i is made bigger slowly until the system is unstable. When k_i rises to 0.0045, the controller loses its function. Attributed to the limitation of the output of the controller, I_3 does not diverge to infinite and it is shown in Fig. 9(c). Under this condition, I_a distorts seriously and the amplitude of I_3 is nearly 10A. It should be noted that the selection of k_i under these two conditions meet the principle (a) and (c) proposed in the previous section. However, when k_i is set at 0.0045, the second component, namely the disturbance in (27) is also bigger than that when k_i is 0.003 and this causes the breakdown of the controller, which means that improving k_i is not beneficial to the stability of the controller. When k_i is between 0.003 and 0.0045, the output of the controller begins to oscillate. Consequently, the maximum of k_i, namely k_{imax} to ensure the normal function of the controller is 0.003 under this condition.

$$k_i = 2\mu k_1 \tag{30}$$

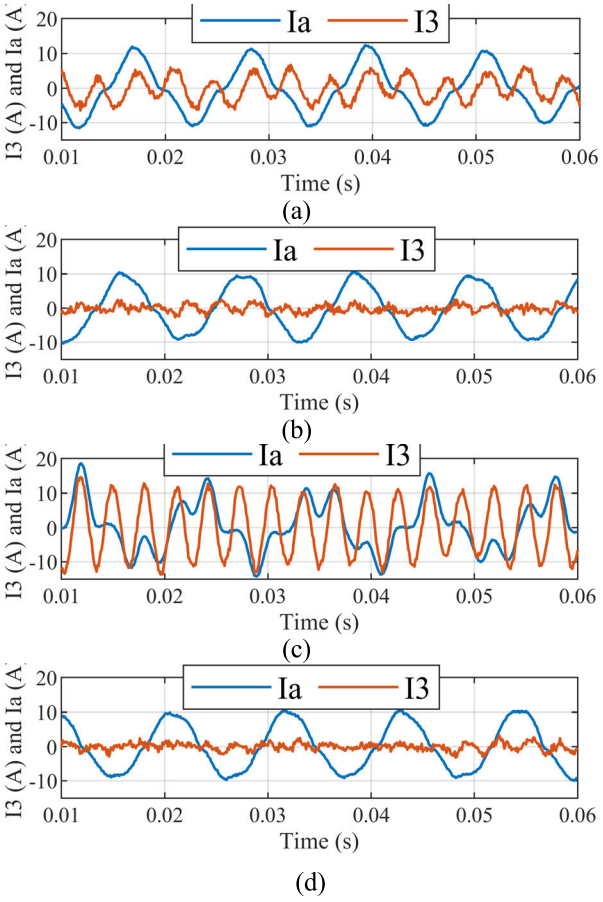

FIGURE 9. steady waveform of I_a and I_3 under different conditions. (a) without I3 suppression; (b) with I3 controller based on LMS and k_i =0.003; (c) with I3 controller based on LMS and k_i =0.0045; (d) with the improved I3 controller where k_p =0.1 and k_i =0.0045.

As to the last condition, the improved controller is enabled. When k_p equals 0.1 and k_i equals 0.0045, waveforms of I_a and I_3 are shown in the fourth figure in Fig. 9. It can be observed that the controller works normally and I_3 is nearly zero, which indicates that the introduction of k_p broadens the steady range

of k_i. This can be explained by (29). k_p helps speed up the attenuation of $V(t)$. the disturbance will decay quickly and has less influence on the improved controller, which makes it possible to select bigger k_i. In the same manner, we can find the k_{imax} under this condition. When k_i rises to 0.024, waveforms of I_a and I_3 begin to vibrate. Namely, k_{imax} of the improved controller is 0.024 under this condition, which is 8 times of that in the traditional controller.

In order to make it clear the influence of k_p on the value range of k_i, k_{imax} under different motor speeds and different k_p are acquired via experiments. The results are shown in Fig. 10 and Fig. 11. It can be observed from Fig. 10 that k_{imax} rises with k_p whatever the motor speed is. Besides, when k_p is smaller than 0.06, k_{imax} has a relatively big rise rate. when k_p exceeds 0.06, the rising rate of k_{imax} slows down, which indicates that with the rise of k_p, the ability of k_p to broaden the steady range of k_i is weak down. Fig. 11 shows the relation between k_{imax} and motor speed. Obviously, when motor speed rises, k_{imax} becomes smaller no matter what k_p is, which can be explained by (29). In the former analysis, the last component of (29) which can also be seen as the disturbance is neglected on the condition that motor speed is small. However, when motor speed rises, the difference of the input signal between the two next sample times becomes bigger, which makes it unreasonable to ignore the last component of (29). Then this component will bring disturbance into the iteration formula of $V(t)$ and finally causes the steady range of k_i to become narrow. For the same reason, it can be inferred that if the control cycle rises, k_{imax} will also become smaller.

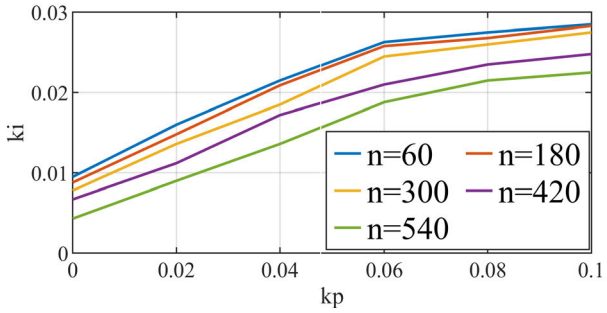

FIGURE 10. relation between k_i and k_p.

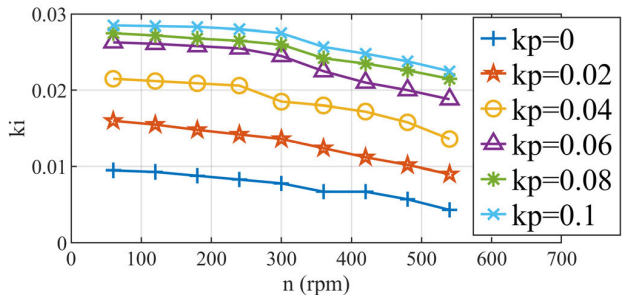

FIGURE 11. relation between k_i and speed.

B. DYNAMIC PERFORMANCE

In order to invest the influence of k_p and k_i on the dynamic response of the improved controller, four groups of experiments are conducted. The motor operates at 540rpm and I_d equals -15A. Then the improved controller with different control parameters is enabled at time 0.06s and I_3 are recorded just as shown in Fig. 12. By comparing Fig. 12(a) and Fig. 12(b), it can be found that I_3 uses shorter time to decrease to zero in the latter, which indicates that increasing k_i can help the controller get a high-speed dynamic response. In the same manner, by making a comparison between Fig. 12(a) and Fig. 12(c) or Fig. 12(b) and Fig. 12(d), it can be concluded that a big k_p is also helpful to improve the dynamic performance of the controller. Besides, when k_p is set at 0.1, I_3 decreases to zero quickly no matter k_i is 0.003 or 0.0005 and it is hard to compare the dynamic performance of the controller under these two conditions. In fact, when k_p exceeds 0.02, the way to improve the dynamic performance by increasing k_i is not rather significant. Namely, among most of the value range of k_p, k_p plays the role to provide a high-speed dynamic response of the controller. k_i does help to eliminate the steady error, which coincides with the analysis in the former. Therefore, k_p and k_i are finally set at 0.1 and 0.0005. This combination can ensure that the controller has a high-speed dynamic performance, a relatively wide range of motor operations and nearly zero steady error at the same time.

The current loop and speed loop are the two main basic control loops in the motor drive control system. Considering this, it is necessary to ensure that the controller still has a satisfactory performance in terms of I_3 elimination when there is a current step or speed step. Then two groups of experiments are conducted and the results are shown in Fig. 13 and Fig. 14. In both two groups of experiments, the traditional controller and the improved controller are enabled respectively. When the control system adopts the traditional controller, k_i is set at 0.003 to ensure that the controller has the best dynamic performance. In the first group of experiments, the motor operates at 540rpm. Then I_d steps from -5A to -15A at time t_1. It can be observed from Fig. 13 that waveforms of I_d under the function of two kinds of controllers are almost the same. Nonetheless, there is a relatively big ripple in the waveform of I_3 when using the traditional controller. When I_d steps from -5A to -15A, the balance between the voltage output by the controller and the harmonic voltage generating I_3 is broken. I_3 increases consequently. Then the controller begins to work and finds the new balance to eliminate I_3. Before the controller finds this new balance, I_3 will flow in phase windings and behaves as ripples in the waveform of itself. When the improved controller is enabled, I_3 remains its value before and after I_d steps and there is nearly no ripple in the waveform of I_3, which means that the improved controller finds the new balance immediately when I_d steps.

In the second group of experiments, I_d is set at -15A. When motor speed steps from 300rpm to 600rpm just as

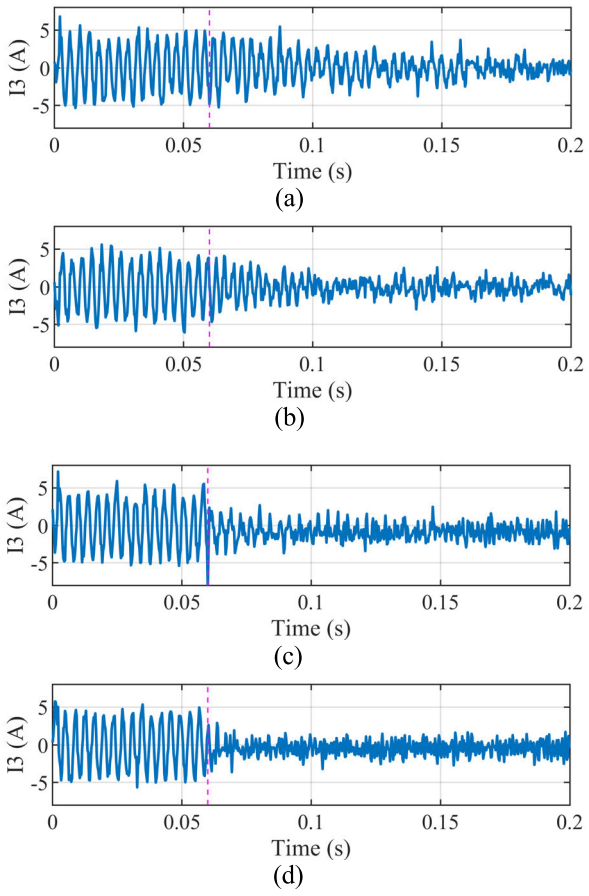

FIGURE 12. dynamic waveform of I_3 under different conditions. (a) k_p =0.01 and k_i =0.0005; (b) k_p =0.01 and k_i =0.003; (c) k_p =0.1 and k_i =0.0005; (d) k_p =0.1 and k_i =0.003.

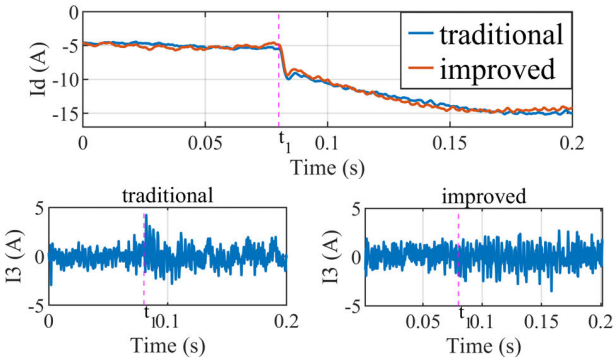

FIGURE 13. transient waveforms of I_d and I_3 under the function of the traditional controller and the improved controller.

shown in Fig. 14. Waveforms of the motor speed, I_d and I_q under the function of two kinds of controllers are nearly the same. However, there is still a big ripple in the waveform of I_3 when the traditional controller is adopted. The reason is similar with that when I_d steps. When the improved controller is enabled, I_3 is quite small even when motor speed steps, which attributes to the high convergence speed of the improved controller.

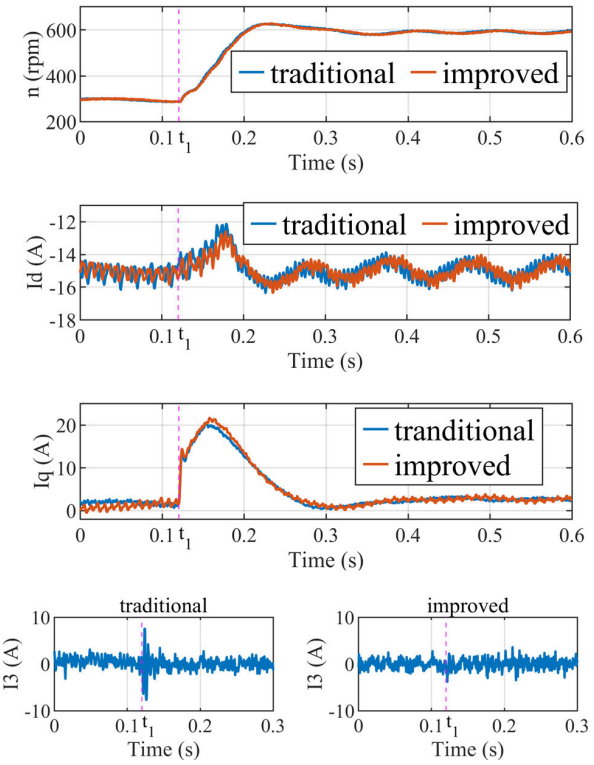

FIGURE 14. transient waveforms of motor speed, I_d, I_q and I_3 under the function of the traditional controller and the improved controller.

V. CONCLUSION

In this paper, the current controller based on LMS and its improved version is proposed and compared. They both can effectively eliminate the third harmonic current when motor operates under a steady state. Besides, the selection principle of control parameters for these two controllers is given and analyzed. According to the analysis and experiment results, some conclusions can be drawn:

1) In general, compared with the controller based on LMS, the improved controller has a wider range of motor operation and an advantage in terms of system stability;
2) The improved controller has a better dynamic performance than the controller based on LMS;
3) In terms of the selection of control parameters, k_p mainly plays the role to offer better dynamic performance and k_i does good to eliminate steady error. Besides, a big k_p can help broaden the value range of k_i. With the rise of the motor speed or control cycle, k_{imax} becomes small. Consequently, it is always appreciated to choose a relatively big k_p and relatively small k_i on the condition that the system is stable.

ACKNOWLEDGMENT

This work was supported by Prof. Liao.

REFERENCES

[1] E. Levi, "Multiphase electric machines for variable-speed applications," *IEEE Trans. Ind. Electron.*, vol. 55, no. 5, pp. 1893–1909, May 2008, doi: 10.1109/TIE.2008.918488.

[2] C. Chen, H. Zhou, G. Wang, and G. Liu, "Unified decoupling vector control of five-phase permanent-magnet motor with double-phase faults," *IEEE Access*, vol. 8, pp. 152646–152658, 2020, doi: 10.1109/ACCESS.2020.3017541.

[3] B. Tian, G. Mirzaeva, Q.-T. An, L. Sun, and D. Semenov, "Fault-tolerant control of a five-phase permanent magnet synchronous motor for industry applications," *IEEE Trans. Ind. Appl.*, vol. 54, no. 4, pp. 3943–3952, Jul. 2018, doi: 10.1109/TIA.2018.2820060.

[4] H. Lu, J. Li, R. Qu, D. Ye, and Y. Lu, "Fault-tolerant predictive control of six-phase PMSM drives based on pulsewidth modulation," *IEEE Trans. Ind. Electron.*, vol. 66, no. 7, pp. 4992–5003, Jul. 2019, doi: 10.1109/TIE.2018.2868264.

[5] J. Karttunen, S. Kallio, P. Peltoniemi, P. Silventoinen, and O. Pyrhonen, "Decoupled vector control scheme for dual three-phase permanent magnet synchronous machines," *IEEE Trans. Ind. Electron.*, vol. 61, no. 5, pp. 2185–2196, May 2014, doi: 10.1109/TIE.2013.2270219.

[6] W. N. W. A. Munim, M. J. Duran, H. S. Che, M. Bermúdez, I. G.-Prieto, and N. A. Rahim, "A unified analysis of the fault tolerance capability in six-phase induction motor drives," *IEEE Trans. Power Electron.*, vol. 32, no. 10, pp. 7824–7836, Oct. 2017, doi: 10.1109/TPEL.2016.2632118.

[7] S. Ding, W. Chen, M. Tong, F. Xie, and C. Zheng, "Fault tolerant control for a five-phase permanent magnet synchronous machine driving system," in *Proc. IEEE 11th Conf. Ind. Electron. Appl. (ICIEA)*, Heifei, China, Jun. 2016, pp. 2021–2025.

[8] J. Huang, P. Zheng, Y. Sui, J. Zheng, Z. Yin, and L. Cheng, "Third harmonic current injection in different operating stages of five-phase PMSM with hybrid single/double layer fractional-slot concentrated winding," *IEEE Access*, vol. 9, pp. 15670–15685, 2021, doi: 10.1109/ACCESS.2021.3052558.

[9] G. Feng, C. Lai, M. Kelly, and N. C. Kar, "Dual three-phase PMSM torque modeling and maximum torque per peak current control through optimized harmonic current injection," *IEEE Trans. Ind. Electron.*, vol. 66, no. 5, pp. 3356–3368, May 2019, doi: 10.1109/TIE.2018.2854550.

[10] B. C. Mecrow, A. G. Jack, J. A. Haylock, and J. Coles, "Fault-tolerant permanent magnet machine drives," in *Proc. Int. Conf. Electr. Mach. Drives*, Durham, U.K., 1995, pp. 433–437.

[11] N. Bianchi, S. Bolognani, and M. D. Pré, "Design and tests of a fault-tolerant five-phase permanent magnet motor," in *Proc. 37th IEEE Power Electron. Spec. Conf.*, Jeju, South Korea, Jun. 2006, pp. 1–8.

[12] H. Zhan, Z.-Q. Zhu, and M. Odavic, "Analysis and suppression of zero sequence circulating current in open winding PMSM drives with common DC bus," *IEEE Trans. Ind. Appl.*, vol. 53, no. 4, pp. 3609–3620, Jul. 2017, doi: 10.1109/TIA.2017.2679678.

[13] F. Wu, H. Ge, and A. EL-Refaie, "Partially-coupled d-q-0 components of magnetically-isolated FSCW IPM machines in Pre- and post-fault control," in *Proc. IEEE Energy Convers. Congr. Expo. (ECCE)*, Portland, OR, USA, Sep. 2018, pp. 269–276.

[14] N. Bodo, M. Jones, and E. Levi, "A space vector PWM with common-mode voltage elimination for open-end winding five-phase drives with a single DC supply," *IEEE Trans. Ind. Electron.*, vol. 61, no. 5, pp. 2197–2207, May 2014, doi: 10.1109/TIE.2013.2272273.

[15] W. Hu, H. Nian, and D. Sun, "Zero-sequence current suppression strategy with reduced switching frequency for open-end winding PMSM drives with common DC BUS," *IEEE Trans. Ind. Electron.*, vol. 66, no. 10, pp. 7613–7623, Oct. 2019, doi: 10.1109/TIE.2018.2881945.

[16] Q. Lu, Y. Zuo, T. Zhang, and L. Mo, "Zero-sequence current suppression for open-winding permanent magnet brushless motor driving system based on second order generalized integrator," *IEEE Access*, vol. 8, pp. 37465–37473, 2020, doi: 10.1109/ACCESS.2020.2975126.

[17] A. G. Yepes, F. D. Freijedo, J. D. Gandoy, O. Lopez, J. Malvar, and P. F. Comesana, "Effects of discretization methods on the performance of resonant controllers," *IEEE Trans. Power Electron.*, vol. 25, no. 7, pp. 1692–1712, Jul. 2010, doi: 10.1109/TPEL.2010.2041256.

[18] A. G. Yepes, F. D. Freijedo, O. Lopez, and J. Doval-Gandoy, "High-performance digital resonant controllers implemented with two integrators," *IEEE Trans. Power Electron.*, vol. 26, no. 2, pp. 563–576, Feb. 2011, doi: 10.1109/TPEL.2010.2066290.

[19] X. Song, B. Han, S. Zheng, and S. Chen, "A novel sensorless rotor position detection method for high-speed surface PM motors in a wide speed range," *IEEE Trans. Power Electron.*, vol. 33, no. 8, pp. 7083–7093, Aug. 2018, doi: 10.1109/TPEL.2017.2753289.

[20] T. D. Batzel and K. Y. Lee, "An approach to sensorless operation of the permanent-magnet synchronous motor using diagonally recurrent neural networks," *IEEE Trans. Energy Convers.*, vol. 18, no. 1, pp. 100–106, Mar. 2003, doi: 10.1109/TEC.2002.808386.

[21] Z. Pan, F. Dong, J. Zhao, L. Wang, H. Wang, and Y. Feng, "Combined resonant controller and two-degree-of-freedom PID controller for PMSLM current harmonics suppression," *IEEE Trans. Ind. Electron.*, vol. 65, no. 9, pp. 7558–7568, Sep. 2018, doi: 10.1109/TIE.2018.2793232.

[22] J.-C. Hwang and H.-T. Wei, "The current harmonics elimination control strategy for six-leg three-phase permanent magnet synchronous motor drives," *IEEE Trans. Power Electron.*, vol. 29, no. 6, pp. 3032–3040, Jun. 2014, doi: 10.1109/TPEL.2013.2275194.

[23] H. S. Che, E. Levi, M. Jones, W.-P. Hew, and N. A. Rahim, "Current control methods for an asymmetrical six-phase induction motor drive," *IEEE Trans. Power Electron.*, vol. 29, no. 1, pp. 407–417, Jan. 2014, doi: 10.1109/TPEL.2013.2248170.

[24] D. Yazdani, A. Bakhshai, and P. K. Jain, "A three-phase adaptive notch filter-based approach to harmonic/reactive current extraction and harmonic decomposition," *IEEE Trans. Power Electron.*, vol. 25, no. 4, pp. 914–923, Apr. 2010, doi: 10.1109/TPEL.2009.2036621.

[25] R. R. Pereira, C. H. da Silva, L. E. B. da Silva, G. Lambert-Torres, and J. O. P. Pinto, "New strategies for application of adaptive filters in active power filters," *IEEE Trans. Ind. Appl.*, vol. 47, no. 3, pp. 1136–1141, May 2011, doi: 10.1109/TIA.2011.2125931.

YIXIAO FENG was born in Henan, China, in 1992. He received the B.Sc. degree in electrical engineering from Chongqing University, Chongqing, China, in 2014, where he is currently pursuing the Ph.D. degree. His current research interests include fault-tolerant control and harmonic elimination of multiphase PM motors.

YONG LIAO received the M.Eng. degree in electrical machinery and the Ph.D. degree in power system control from Chongqing University, Chongqing, China, in 1988 and 1997, respectively. From 2001 to 2002, he was a Visiting Professor at Northumbria University, Newcastle, U.K. He is currently a Professor of electrical machinery and apparatus at Chongqing University. In 1998, he participated in the Global Development Program of Rockwell Automation, Milwaukee, WI, USA. His research interests include the control of doubly-fed electrical machines as used in renewable energy systems, including wind and micro-hydro generators.

XUEKE ZHANG received the B.S. degree in electrical engineering from Zhengzhou University, Zhengzhou, China, in 2014, where she is currently pursuing the master's degree. Meanwhile, she is also a staff in Xinxiang Power Supply Company, State Grid Henan Electric Power Company.

Her current research interest includes the fault-tolerant motor design.